Analysis of the decay of molecular fluorescence in optically excited mercury vapor[a)]

M. Stock,[b)] E. W. Smith, R. E. Drullinger, M. M. Hessel, and J. Pourcin[c)]

Laser Physics Section, National Bureau of Standards, Boulder, Colorado 80302
(Received 3 October 1977)

The decay of the 485 and 335 nm molecular fluorescence bands in optically excited mercury vapor is studied. A 10 nsec laser pulse at 256 nm is used to excite the vapor and the subsequent fluorescence intensity between 1 and 2000 μsec was recorded for each band. At late times following the laser pulse, both bands decay at the same exponential rate. This exponential decay coefficient was measured as a function of gas density from 10^{17} to 10^{19} cm^{-3} and as a function of temperature from 473 to 1048°K. These decay data, as well as data on the relative intensities of the two bands, are analyzed in terms of a simple kinetic model for the mercury vapor system and various kinetic rates are determined. Some decay rates for the 6^3P atomic manifold are also obtained and compared with previous measurements.

INTRODUCTION

In previous papers[1,2] an analysis was made of the potential energy curves and transition A values for the excited molecular states of mercury which give rise to the 335 and 485 nm fluorescence bands. Calculations of other excited molecular states were discussed[2,3] and experimental evidence for theoretically predicted low lying metastable molecular states (gerade states) was obtained by absorption of infrared laser radiation.[4]

In the present paper we report measurements of the decay of the 335 and 485 nm molecular fluorescence bands following optical excitation of mercury vapor by a 10 nsec pulse pulse of 256 nm laser radiation. Some transient behavior is observed immediately following the laser pulse but at sufficiently late times both fluorescence bands decay exponentially in time with the same decay coefficient. This exponential decay coefficient was measured for gas densities from 10^{17} to 10^{19} cm^{-3} at temperatures from 473 to 1048 °K.

A simple kinetic model is developed for the excited states which can explain the temperature and density dependence of this decay coefficient as well as previous measurements[1,2,5] of the ratio of fluorescence band intensities. Various kinetic rates are obtained for this model, including some atomic decay rates which are compared with previous measurements.[6]

II. EXPERIMENTAL PROCEDURE AND RESULTS

The molecular fluorescence was excited by tuning a pump laser off resonance on the red side of the 253.7 nm atomic resonance line $6^1S_0 \rightarrow 6^3P_1$. This excites Hg_2 molecules in high vibrational levels of the 1_u state (Fig. 1). Some of this excitation is vibrationally stabilized directly to low lying states, some is reradiated at the pump laser wavelength, and, since our pump wavelength 256 nm lies within kT of the 253.7 nm resonance line, some excitation produces 6^3P_1 atoms. However, for mercury atom densities above 10^{17} cm^{-3} more than 90% of this excitation is converted into metastable 6^3P_0 atoms[6] due to rotational mixing of the 1_u and 0_u^- states at small internuclear separations (see Fig. 1). The decay of these metastable atoms has been studied[6] and it is known that they form mercury molecules by three body recombination with a rate coefficient of 1.6×10^{-31} $cm^{-6}\,sec^{-1}$. This recombination is the source for the molecular fluorescence at late times following the exciting laser pulse.

The measurement system shown in Fig. 2 consisted of a pump laser system, a heated sample cell containing pure mercury, and a fast detection system for averaging and storing the fluorescence signal.

The pump laser is the same as that used in Ref. 6. A commercial nitrogen laser (180 kW, 10 nsec pulse)

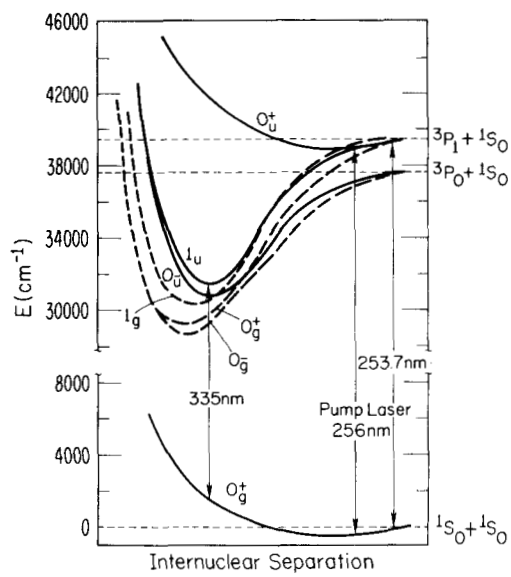

FIG. 1. Theoretical estimates of several low lying Hg_2 potential curves based on *ab initio* calculations[3] for Mg_2 and experimental observations[1,2] on Hg_2. The pump laser absorption is shown as well as the center of the 335 nm molecular fluorescence band. The 485 nm fluorescence band arises from Hg_3 and is thus not shown in this figure.

[a)]Supported in part by ERDA Contract #*E*(49-1)-3800 and by ARPA Order # 891, Amendment 11.

[b)]Postdoctoral Research Fellow supported by the Deutsche Forschungs Gemeinschaft. Present address: Universität Kaiserslautern, Fachbereich Physik, 675 Kaiserslautern, West Germany.

[c)]On leave from the Université de Provence, Marseille, France.

 0021-9606/78/6804-1785$01.00

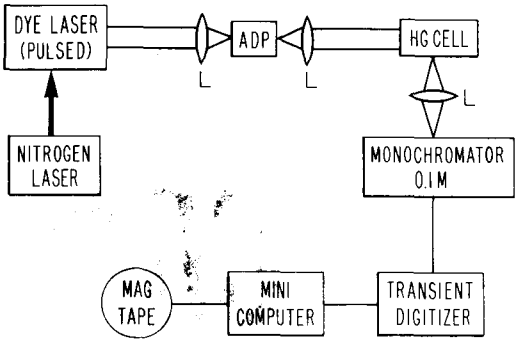

FIG. 2. Schematic diagram of the apparatus.

was used to pump a dye laser built in the Hänsch configuration employing a dye cell, beam expanding telescope, grating for tuning wavelength, Glan-Thompson polarizer, and end mirror with 40% transmission. With a coumarin dye the dye laser produced a 50 kW, 10 nsec pulse at 512 nm with a spectral width of 0.03 nm. This laser beam was frequency doubled in a temperature tuned ADP crystal and the uv output was separated from the visible beam with a quartz prism. The resulting 15 kW, 10 nsec, 256 nm laser pulse was then used to excite the $6\,^3P_0$ atoms as discussed above.

The sample cell was also the same as that discussed in Ref. 6; a quartz tube 5 cm long by 3 cm in diameter heated in a brick oven with the temperature controlled to within a few hundredths of a degree. A small tube extending vertically downward into a lower oven served as the mercury reservoir. The lower oven was separately heated and maintained at a temperature below that of the upper oven, thus permitting independent control of both temperature and density within the sample cell. Purity of the mercury vapor is critical for decay measurements; the distilling and cell filling procedures employed are discussed in Ref. 8.

The detection system consisted of a fast 0.1 m monochromator (2.0 nm resolution) coupled to a transient digitizer (8 bit, 2000 channel) which recorded the time history of the fluorescence following each pump laser pulse and a minicomputer to average subsequent shots. The averaged signals were stored on a magnetic tape as a function of fluorescence wavelength for later analysis on a larger computer.

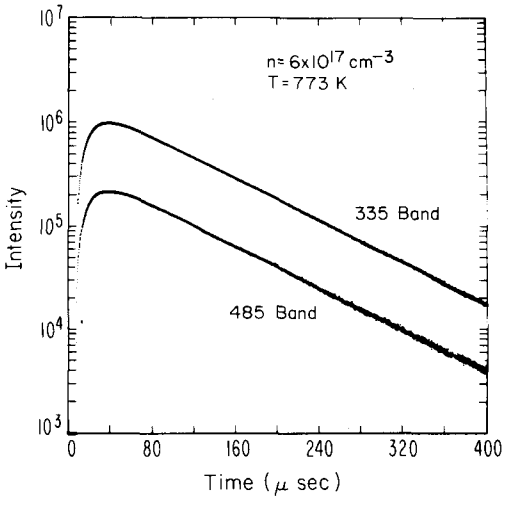

FIG. 3. Fluorescence intensity versus time illustrating the general behavior for densities above 3×10^{17} cm^{-3} and temperatures above 600 °K. Note that both bands decay together at late times.

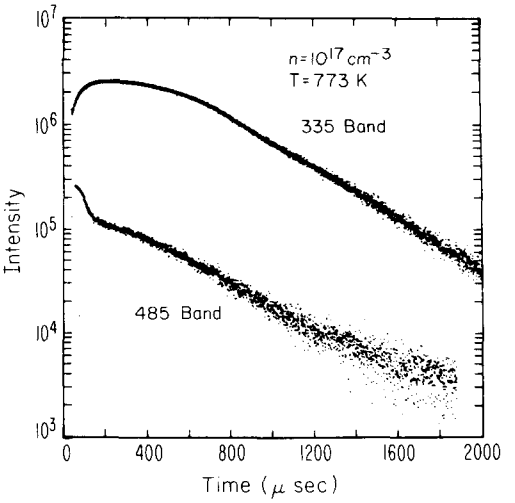

FIG. 4. Fluorescence intensity versus time for a low density $n=10^{17}$ cm^{-3} and a high temperature $T=773$ °K, illustrating transient behavior at early times. Both bands decay together at late time $t>800$ μsec but the 485 nm intensity becomes very weak and unreliable for $t>1400$ μsec.

Decay measurements were made at various wavelengths within the two prominent mercury fluorescence bands centered near 335 and 485 nm. At late times following the laser pulse all wavelengths in both bands exhibited the same decay rate. Typical high density traces are shown in Fig. 3. Both bands rise very quickly following the laser pulse and decay together exponentially; this general behavior is observed for all temperatures at the higher densities. At low densities, Figs. 4 and 5, the bands decay together only at very late times. At earlier times the 485 nm band shows an initial fast decay followed by a slower decay component or, at low enough temperatures, an increase in intensity which then goes over, at late times, to the same exponential decay rate as the 335 nm band.

In this paper we have analyzed only the final exponential decay component when both 335 and 485 nm bands decay together. The exponential decay coefficient γ is plotted as a function of temperature and density in Fig. 6 and a comparison with the data of Matland and McCoubrey[5] is given in Fig. 7. The solid curves in Figs. 6 and 7 show our fit to the data using the model discussed in the following section. The estimated uncertainty of the data for densities above 10^{17} cm^{-3} are $\pm10\%$ (error bars not shown), whereas the error bars are $\pm20\%$ for $n=10^{17}$ cm^{-3} since the signal was much weaker resulting in a lower signal to noise ratio.

III. DISCUSSION OF MODEL

The data given in Fig. 6 were analyzed in terms of a simple model for the low lying atomic and molecular

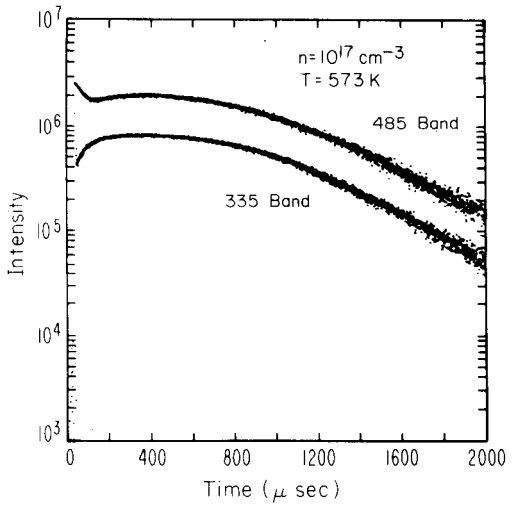

FIG. 5. Fluorescence intensity for a low density and low temperature illustrating transient behavior in which the 485 nm band undergoes an initial rise and decay ($t > 150$ μsec) followed by a second rise ($150 < t < 400$ μsec) and subsequent decay at late times ($t > 800$ μsec). Both bands decay together in the final decay mode at late times.

states and various rate coefficients were determined based on this model. Actually several other models were tried and rejected since they were unable to explain one or more aspects of the observed data; these will be discussed when they bear on the data.

The model finally used had four states as shown in Fig. 8. An atomic state labeled 0 was included to represent the $6\,^3P_0$ state which is excited by the pump laser. The state 1 represents the doubly degenerate 1_u state of Hg_2 which radiates the 335 nm band.[1,2] It is expected that one or more of the $0_g^{\pm}$ metastable states lie below the 1_u state (see Fig. 1) since Mosburg and Wilke[4] were able to pump such a transition using the 2.8–3.0 μm output of an HF laser; the state 2 represents the metastable state with the lowest energy (the others cannot be detected by the present analysis). Finally, the state 3 represents a stable Hg_3 state which emits the 485 nm band. This trimer state may dissociate to either of the dimer states 1 and 2.

The differential equations describing the time development of the population densities n_i may be expressed by the matrix equation

$$\frac{d}{dt}\begin{bmatrix} n_0 \\ n_1 \\ n_2 \\ n_3 \end{bmatrix} = \begin{bmatrix} -\gamma_0 & R_{01} & R_{02} & 0 \\ r_{10} & -\gamma_1 & R_{12} & R_{13} \\ r_{20} & R_{21} & -\gamma_2 & R_{23} \\ 0 & r_{31} & r_{32} & -\gamma_3 \end{bmatrix} \begin{bmatrix} n_0 \\ n_1 \\ n_2 \\ n_3 \end{bmatrix} + \begin{bmatrix} P(t) \\ 0 \\ 0 \\ 0 \end{bmatrix} \tag{3.1}$$

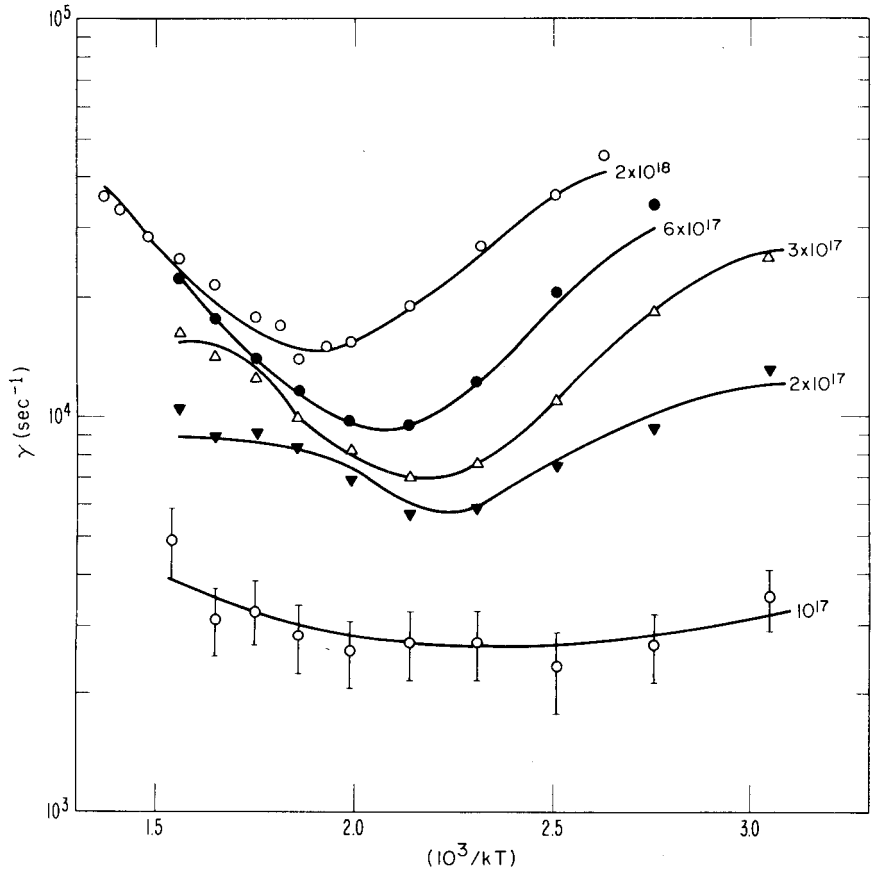

FIG. 6. Exponential decay coefficient for decay at late times as a function of temperature (kT is in cm^{-1}) for a few representative densities. Estimated errors of ±10% for $n \geq 2\times10^{17}$ cm^{-3} are not shown for the sake of clarity. The ±20% error in the $n = 10^{17}$ cm^{-3} data are due to a lower signal to noise ratio at low densities. Solid lines represent calculations with our theoretical model.

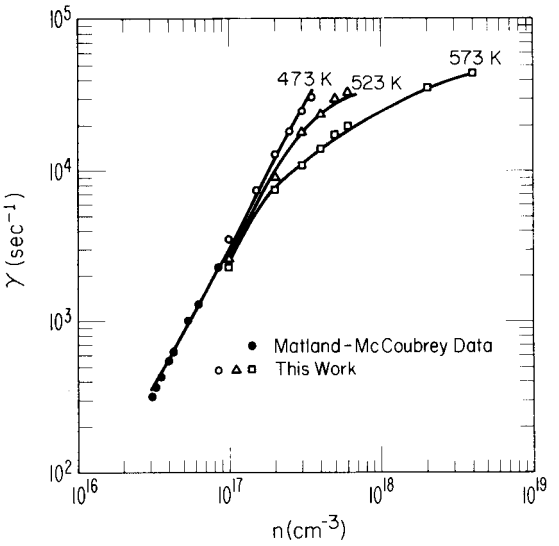

FIG. 7. Exponential decay coefficient for decay at late times as a function of density for three low temperatures. The 473 °K data of Matland and McCoubrey[5] are included, showing that the decay coefficient approaches a density squared asymptote for low temperatures. Solid curves represent calculations with our theoretical model. According to the model, this low temperature asymptote is the molecular formation rate due to three body recombination of $6\,^3P$ and $6\,^1S_0$ atoms.

where R_{ij} and r_{ij} denote two body and three body inelastic collision rates from state j to state i. The terms γ_i represent the loss rates

$$\gamma_1 = A_{335} + R_{01} + R_{21} + r_{31} \ , \tag{3.2}$$

$$\gamma_2 = R_{02} + R_{12} + r_{32} \ , \tag{3.3}$$

$$\gamma_3 = A_{485} + R_{23} + R_{13} \ , \tag{3.4}$$

where A_{335} and A_{485} represent the A values for emission of the 335 and 485 nm bands, respectively. Actually, the A values for these bands depend on the vibrational quantum number but the inclusion of vibrational states is beyond the scope of our simple kinetic model; these A values should therefore be regarded as vibrationally averaged effective A values. At late times most of the vibrational population resides in lower vibrational levels; hence, these effective A values will be strongly weighted toward lower quantum numbers which correspond to the centers of the emission bands. The decay rate γ_0 for the atomic state is known from previous work[6] but it was nontheless treated as unknown in order to provide a check on the values obtained in Ref. 6. Diffusion losses were evaluated theoretically using known diffusion coefficients[9,10] and diffusion terms were also included in early versions of our kinetic model, but they were found to be negligible for the densities considered in this paper. Quenching of the dimer and trimer by collision induced transitions to the electronic ground state was also ignored because the collision partner (i.e., atomic mercury) is not expected to produce any low lying potential energy curve crossings which might enhance such cross sections. Collisional dissociation of the dimer and trimer are thus expected to be several orders of magnitude faster than quenching to the ground state.

The exponential decay coefficient for the decay of the fluorescence at late times is the smallest eigenvalue of the 4×4 matrix in Eq. (3.1). In general, the eigenvalues of this matrix are the solutions of a quartic equation for the roots γ. This may be reduced to an analytically soluble problem by noting that A_{335} is expected to be[2] about, 10^6 sec^{-1} which is much greater than all observed values of the decay coefficient (Fig. 6). We may therefore neglect γ whenever it is added to A_{335}, thereby reducing the eigenvalue problem to a cubic equation of the form

$$0 = \gamma^3 - a_2\gamma^2 + a_1\gamma - a_0 \ . \tag{3.5}$$

Since the energy separation E_{01} between the 0 and 1 states is about 6900 cm^{-1} (see Table II of Ref. 2) and the separation E_{12} between 1 and 2 is expected to be[4] about 2000 to 3000 cm^{-1}, we may assume that $R_{21} \gg R_{01}$, $R_{21} \gg R_{02}$, and $R_{12} \gg R_{02}$. With these assumptions the coefficients in Eq. (3.5) reduce to

$$\begin{aligned} a_2 &= \gamma_0 + A_{485} + R_{23} + r_{32} + d_1[R_{12}(A_{335} + r_{31}) + R_{13}(A_{335} + R_{21})] \\ &= \gamma_0 + \alpha_2 \ , \end{aligned} \tag{3.6}$$

$$\begin{aligned} a_1 &= \gamma_0\alpha_2 + d_1A_{335}R_{12}[A_{485} + R_{23} + d_1R_{13}(A_{335} + R_{21})] \\ &\quad + r_{32} + d_1r_{31}R_{12})(A_{485} + d_1A_{335}R_{13}) \\ &= \gamma_0\alpha_2 + \alpha_1 \ , \end{aligned} \tag{3.7}$$

$$a_0 = \gamma_0\alpha_1 \ , \tag{3.8}$$

where

$$d_1 \equiv 1/(A_{335} + R_{21} + r_{31}) \ . \tag{3.9}$$

Recall that γ_0 is the decay rate for the atomic manifold, state 0 in our model, which will be discussed in more detail in Sec. IV.E.

The cubic equation (3.5) is easily solved by the standard method[11] and the smallest of the three real roots is given by

$$\gamma = \frac{|a_2|}{3} - \frac{|a_2|}{3}\sqrt{1 - \frac{3a_1}{a_2^2}}\,(\cos\theta + \sqrt{3}\sin\theta) \ , \tag{3.10}$$

$$\theta = \frac{1}{3}\sin^{-1}\left\{\left[\frac{a_0^2}{4} + \frac{a_0a_2}{27}\left(a_2^2 - \frac{9}{2}a_1\right) - \frac{a_1^2}{108}\,(a_2^2 - 4a_1)\right] \Big/ \left(\frac{a_1}{3} - \frac{a_2^2}{9}\right)^3\right\}^{1/2} . \tag{3.11}$$

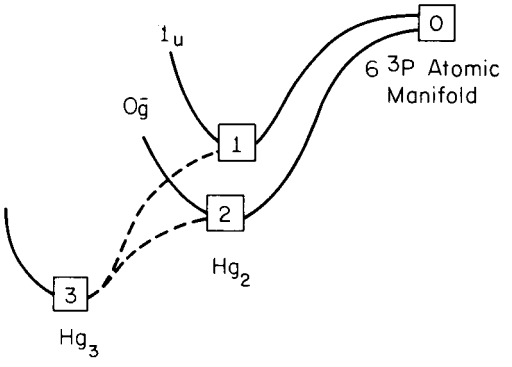

FIG. 8. Schematic diagram of the four states included in our kinetic model.

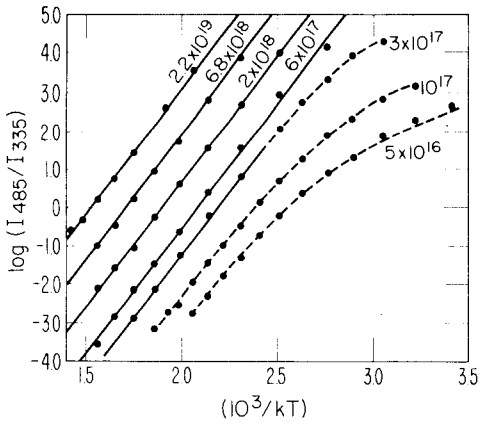

FIG. 9. Ratio of 485 to 335 nm integrated band intensities as a function of temperature for several different densities. The high density, high temperature asymptote (solid lines) is given by the function $I_{485}/I_{335} = 2.2\times10^{-24} n \exp(6500/kT)$, where kT is in cm^{-1}. This Boltzmann factor shows that the two electronic states responsible for the 485 and 335 nm bands are in thermal equilibrium for $n \geq 3\times10^{17}$ cm^{-3} and $T \geq 575$ °K (or $1/kT \leq 2.5\times10^{-3}$ cm). The dashed curve represents our fit to the low temperature low density data discussed in Sec. IV. B.

Substituting Eqs. (3.6)–(3.8) into Eqs. (3.10) and (3.11) gives an expression for γ in terms of the parameters γ_0, A_{335}, A_{485}, k_{21}, k_{23}, K_{32}, K_{31}, k_{13}, E_{12}, E_{23}, and g_2 (the degeneracy of the state 2), where

$$r_{31} = n^2 K_{31} , \tag{3.12}$$

$$r_{32} = n^2 K_{32} , \tag{3.13}$$

$$R_{21} = g_2 n k_{21} , \tag{3.14}$$

$$R_{12} = (2/g_2) n k_{21} \exp(-E_{12}/kT) , \tag{3.15}$$

$$R_{23} = g_2 n k_{23} \exp(-E_{23}/kT) , \tag{3.16}$$

$$R_{13} = 2n k_{13} \exp[-(E_{12}+E_{23})/kT] . \tag{3.17}$$

In addition to the decay data reported in the present paper, we also required that our model fit the steady state measurements of the fluorescence intensity.[1] In Eq. (4.10) of Ref. 2 it was noted that, for densities above 3×10^{17} cm^{-3} and temperatures above 575 °K, the ratio of intensities in the 485 and 335 nm bands may be described by the equation

$$\frac{I_{485}}{I_{335}} = 2.2\times10^{-24} n \exp(6500/kT) , \tag{3.18}$$

where kT is in cm^{-1} and n is the gas density in cm^{-3}. Measurements for lower temperatures and densities were also reported in Fig. 4 of Ref. 2.

In terms of our present model this intensity ratio is given by

$$\frac{I_{485}}{I_{335}} = \left(\frac{A_{485}}{A_{335}}\right)\left(\frac{n_1}{n_3}\right) . \tag{3.19}$$

The steady state population ratio (n_1/n_3) may be obtained from Eq. (3.1) by setting $(dn_i/dt) = 0$ and inverting the 4×4 matrix to yield an equation for the set of n_i. In this manner one obtains

$$\frac{n_1}{n_3} = \frac{R_{12}(A_{485}+R_{23}+R_{13}) + r_{32}R_{13} + \phi r_{32}A_{485}}{(R_{21}r_{32}+r_{31}R_{12}+r_{31}r_{32}) + (1-\phi)r_{32}A_{335}} , \tag{3.20}$$

where

$$\phi = r_{10}/(r_{10}+r_{20}) . \tag{3.21}$$

The four state model discussed above was used to numerically fit the measurements of both the long time decay constant [using Eqs. (3.6)–(3.11)] and the ratio of integrated band intensities [using Eq. (3.20)]. The fits are represented by the solid and dashed curves in Figs. 6, 7, 9, and 10. The parameters determined by these fits are listed in Table I and their accuracy is discussed in Secs. IV.D and IV.E.

An alternate model was tested which included an additional trimer state energetically degenerate with state 2 of the dimer. This trimer state was regarded as an unbound collision complex (lifetime of the order of 10^{-12} sec) which could radiate at 485 nm. This state was used to test the hypothesis that the 485 nm band is emitted by "collision induced" radiation from a metastable dimer rather than a stable trimer. The model with collision induced 485 nm radiation was unable to explain the n^2 density dependence of the ratio of integrated band intensities I_{485}/I_{335} at low densities [see Fig. 10].

IV. ANALYSIS OF DATA

A. Decay rate at high densities

There are basically two energy reservoirs in our four state model, namely, the $6\,^3P_0$ atomic state and the metastable $0_g^{\pm}$ molecular states (represented by the states 0 and 2 in our model). A model with a fifth state representing a low lying metastable trimer level was also tried but no experimental evidence (i.e., temperature dependence at high density, low temperature) could be found to confirm the presence of such a state.

The decay of the molecular fluorescence is thus determined by the decay of these two energy reservoirs. For high densities ($n > 3\times10^{17}$ cm^{-3}) the decay rate γ_0 of the atomic state is known[6] to be much faster than the observed decay rates for the molecular fluorescence. Thus, at these higher densities the observed decay rate must be determined by the rate at which the molecular energy reservoir is emptied.

TABLE I. Atomic and molecular parameters determined by fitting fluorescence decay data and steady state intensity ratios as discussed in Sec. IV. The molecular rate coefficients are indicated pictorially in Fig. 10.

Molecular parameters			Atomic parameters This work	Ref. 6
A_{335}	1.0×10^{6} sec^{-1}			
A_{485}	5.8×10^{4} sec^{-1}	β	2.5×10^{4}	10^{4} sec^{-1}
E_{12}	2800 cm^{-1}	$k_0^{(2)}$	1.5×10^{-13}	2.8×10^{-13} $cm^3\,sec^{-1}$
E_{23}	3800 cm^{-1}	$k_0^{(3)}$	1.8×10^{-31}	1.6×10^{-31} $cm^6\,sec^{-1}$
k_{21}	1.6×10^{-10} $cm^3\,sec^{-1}$	c	1.4	
k_{32}	9.8×10^{-31} $cm^6\,sec^{-1}$	k_q	$<5\times10^{-15}$	4×10^{-14} $cm^3\,sec^{-1}$
k_{23}	1.7×10^{-8} $cm^3\,sec^{-1}$			
$K_{10}/(K_{10}+K_{20})$	0.3			
g_2	1.1			

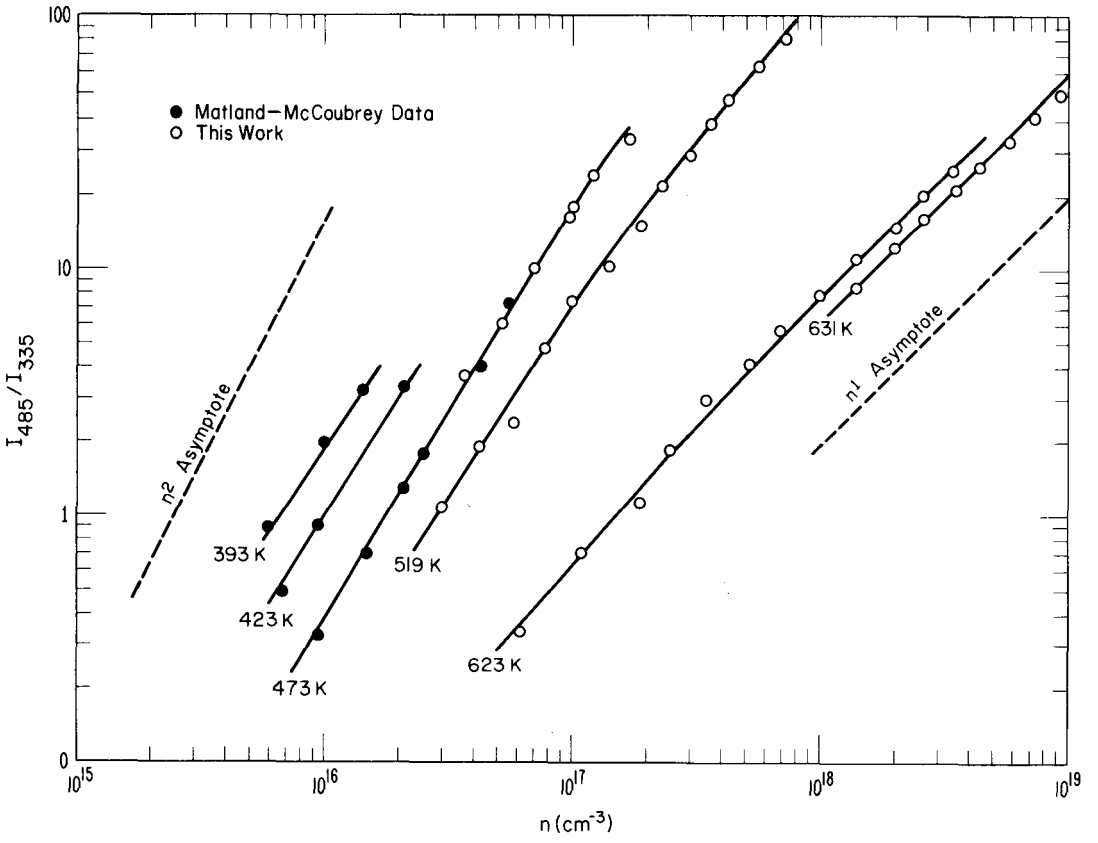

FIG. 10. Ratio of 485 to 335 nm integrated band intensities as a function of density for several representative temperatures. The uncalibrated data of Matland and McCoubrey were calibrated by requiring that they agree with our calibrated data at 473 °K. Notice that the data depend linearly on density at high temperatures and densities (thermal equilibrium region, Fig. 9) and they approach a density squared asymptote for low temperatures and densities. Solid curves represent calculations with our theoretical model.

It is possible to obtain a simplified expression for this purely molecular decay component by expanding Eq. (3.10) in powers of $1/\gamma_0$ (subsequent to the analysis it can be verified that $\gamma_0 \gg \alpha_1$ and $\gamma_0 \gg \alpha_2$). This expansion gives

$$\gamma \simeq \tfrac{1}{2}\alpha_2 - \tfrac{1}{2}\sqrt{\alpha_2^2 - 4\alpha_1}\,. \tag{4.1}$$

Next, using the definitions of α_1 and α_2 in Eqs. (3.6) and (3.7) and noting that $\alpha_2^2 > 4\alpha_1$ we have

$$\begin{aligned}\gamma &\simeq \alpha_1/\alpha_2 \\ &= \gamma_{335} + \gamma_{485}\end{aligned} \tag{4.2}$$

where

$$\gamma_{335} \equiv A_{335}(d_1/\alpha_2)[R_{12}(A_{485} + R_{23} + R_{13}) + r_{32}R_{13} + \phi r_{32}A_{335}]\,, \tag{4.3}$$

$$\gamma_{485} \equiv A_{485}(d_1/\alpha_2)[r_{31}R_{12} + r_{32}(R_{21} + r_{31}) + (1-\phi)r_{32}A_{335}]\,. \tag{4.4}$$

Comparing with Eq. (3.20) we see that these terms have the property

$$\gamma_{335}/\gamma_{485} = A_{335}n_1/A_{485}n_3 = I_{335}/I_{485}\,, \tag{4.5}$$

that is, at high densities, where the decay of the atomic energy reservoir has no influence on the decay of the system, the observed decay reduces to a sum of two terms γ_{335} and γ_{485}. Furthermore, the ratio of these two terms equals the integrated 335 and 485 nm band intensities. These two decay components are thus interpreted as the rates at which the metastable dimer state (state 2 in our model) decays via the 335 and 485 nm emission channels respectively.

It is possible to extract these two decay components from the experimental data by expressing each observed value of γ as the sum of two terms whose ratio is I_{335}/I_{485}. This ratio is very well known from previous measurements of integrated band intensities and is given by Eq. (3.18). The 335 and 485 nm decay components are plotted separately in Figs. 11 and 12.

For high densities ($n > 3\times10^{17}$ cm^{-3}) we may use the approximations $R_{21} \gg A_{335}$ and $R_{23} \gg A_{485}$. The approximations $R_{21} \gg R_{12}$ and $R_{23} \gg R_{13}$ are also well satisfied for all temperatures of interest due to the exponential factors in Eqs. (3.15)–(3.17). In addition we find that, even at our highest densities, $R_{21} \gg r_{31}$; thus, the theoretical expressions defined in Eq. (4.2) reduce to

$$\begin{aligned}\gamma_{335} &\simeq A_{335}R_{12}/R_{21} \\ &= (2/g_2)A_{335}\exp(-E_{12}/kT)\,,\end{aligned} \tag{4.6}$$

$$\begin{aligned}\gamma_{485} &\simeq A_{485}r_{32}/(R_{23} + r_{32}) \\ &= n(A_{485}k_{32}/k_{23})\exp(E_{23}/kT)/[1 + n(K_{32}/k_{23})\exp(E_{23}/kT)]\,.\end{aligned} \tag{4.7}$$

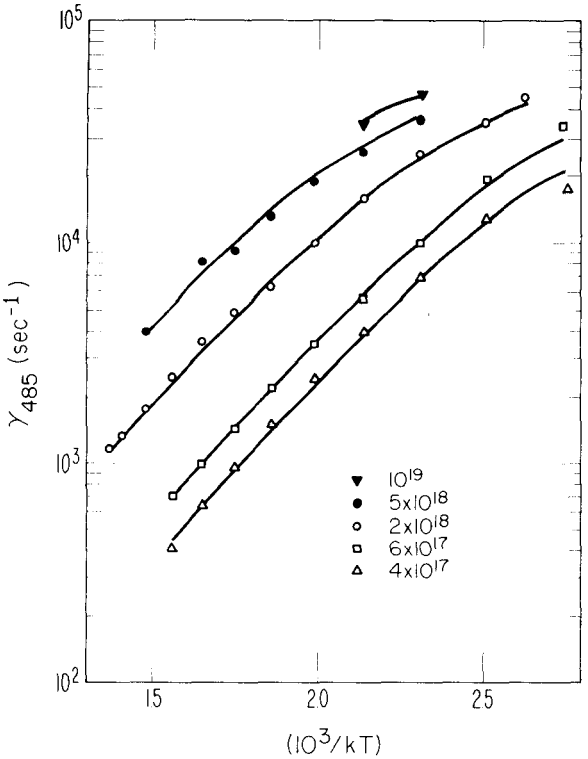

FIG. 12. Rate coefficient γ_{485} for decay via 485 nm radiation as a function of temperature, kT is in cm^{-1}, for several representative densities. The solid curves represent our fit to the data using the kinetic model discussed in Sec. IV.A.

These two expressions fit all the data in Figs. (11) and (12) and thus determine the values of E_{12}, E_{23}, A_{485}, K_{32}/k_{23}, and A_{335}/g_2.

B. Decay rate at low densities

At a density of 10^{17} cm^{-3} the known[6] decay rate for the atomic state γ_0 is slower than the decay of the molecular energy reservoir, state 2. The decay of the molecular fluorescence is therefore controlled by the atomic decay. The transition from the molecular decay component $\gamma_{335}+\gamma_{485}$ at high densities ($n>3\times10^{17}$ cm^{-3}) to the atomic decay component γ_0 at $n=10^{17}$ cm^{-3} is clearly distinguishable in Fig. 6. At the higher densities the observed decay rises sharply with increasing temperature for $T>723$ °K and with decreasing temperature for $T<623$ °K. This is due to the exponential factors in Eqs. (4.6) and (4.7) and it gives the molecular decay component a bowl shaped character which is seen quite clearly at the higher densities. By contrast, the atomic decay, seen most clearly for $n=10^{17}$ cm^{-3}, has a much flatter temperature dependence. For densities in the range 2×10^{17}–4×10^{17} cm^{-3} the molecular decay dominates around 673 °K with the influence of the atomic decay being seen only at the extremes of high and low temperatures. In general, the observed decay is dominated by the smaller of the two decay components. In the density region 2×10^{17}–4×10^{17} cm^{-3} it is thus necessary to use the complete solution of the cubic equation (3.10) in order to fit the measured values of the decay coefficient.

C. Intensity ratio data

Measurements of the decay rate at high densities could be used for a direct determination of several parameters in our kinetic model. However, at low densities the influence of the atomic decay produces more complicated theoretical expressions resulting in a greater uncertainty in the molecular parameters determined by fitting the decay data. This is unfortunate since some parameters become important only at low densities where their determination is thus obscured.

Steady state measurements[1] of the ratio of integrated 485 and 335 nm band intensities are only weakly affected by the atomic state; hence, they may be used at both high and low densities. Our expression for the ratio of integrated band intensities [Eqs. (3.19) and (3.20)], may be simplified by using the approximations $R_{21}\gg R_{12}$, $R_{23}\gg R_{13}$, which are a result of the exponential factors in Eqs. (3.15)–(3.17), and $R_{21}\gg r_{31}$, which is found to hold even for densities as high as 2.2×10^{19} cm^{-3}. With these approximations Eq. (3.20) reduces to

$$\frac{n_1}{n_3}=\frac{R_{12}(A_{335}+R_{23})+\phi r_{32}A_{335}}{r_{32}R_{21}+(1-\phi)A_{335}}\ . \tag{4.8}$$

This expression provides a good fit to all the intensity ratio data as shown in Figs. 9 and 10. Since the values of E_{12}, E_{23}, A_{485}, K_{32}/k_{23}, and A_{335}/g_2 were determined by fitting the decay coefficient, this fit now permits a determination of k_{23}, K_{32}, k_{12}, g_2, and ϕ.

D. Discussion of molecular parameters

The accuracy of molecular parameters in Table I is about ± 10% according to the statistics of our fit. However, this merely indicates that we have achieved a good fit to the experimental data using our kinetic model. The true accuracy of the physical parameters is determined mainly by inadequacies in our kinetic model such as the lack of vibrational states and various approximations to the temperature dependence of the rate coefficients. We estimate that the molecular rate coefficients (except for k_{23} discussed below) and A values are accurate to within a factor of 2; the energies E_{12} and E_{23} seem to be accurate to within ± 10%.

The sum $E_{12}+E_{23}=6600$ cm^{-1} is within 2% of the value 6500 cm^{-1}, which is the known energy separation[2] between the two states which radiate at 485 and 335 nm. It should be mentioned that we also tried a model containing an energy barrier between the dimer state 2 and the trimer state 3. The right hand sides of Eqs. (3.13) and (3.16) were multiplied by $\exp(-\epsilon/kT)$ and the barrier height ϵ was treated as an adjustable parameter. These fits always gave $\epsilon=0$, indicating that no such energy barrier exists.

As mentioned earlier, A_{335} is an effective A value averaged over the vibrational levels of the 1_u state. From Table II of Ref. 2 we see that the A values range from about 7×10^5 sec^{-1} at the bottom of the 1_u well to 1.3×10^6 sec^{-1} for vibrational states lying 450 cm^{-1} (about kT) above the bottom of the well. A thermal average over vibrational states would therefore yield an

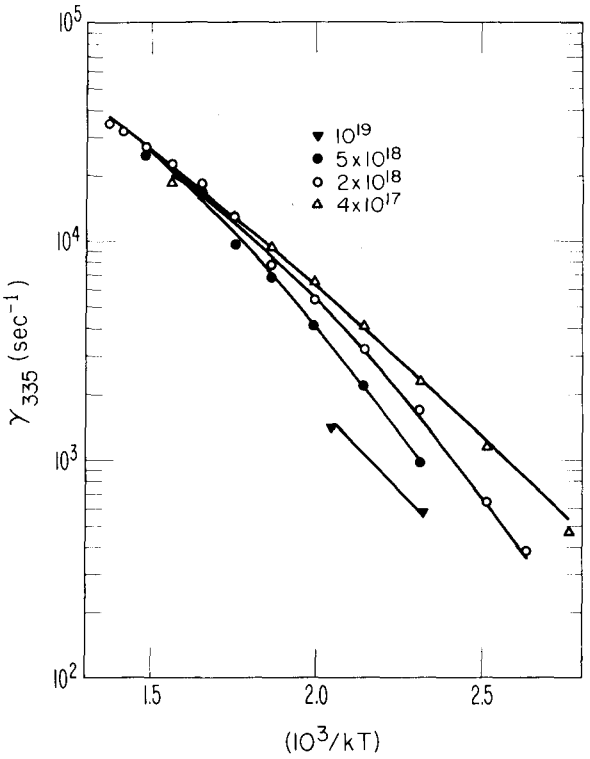

FIG. 11. Rate coefficient γ_{335} for decay via 335 nm radiation as a function of temperature, kT is in cm^{-1}, for several representative densities. The solid curves represent our fit to the data using the kinetic model discussed in Sec. IV.A.

average value very close to our measured value $A_{335} \simeq 10^6$ sec^{-1}. The trimer A value A_{485} is roughly 17 times smaller than that for the radiating dimer state in agreement with the estimate made in Eq. (4.12) of Ref. 2.

The degeneracy g_2 of the metastable dimer state 2 was treated as an adjustable parameter because it was thought that two or more of the low lying gerade states (see Fig. 1) might be degenerate. The best fit to the data was obtained with a degeneracy $g_2 \simeq 1.1$, indicating that the lowest gerade state is not degenerate with any others.

The three body trimer formation rate K_{32} was taken to be independent of temperature even though it is known (Ref. 12, p. 336) that such rates very often decrease with temperature. Such an effect probably represents a factor of 2 change in K_{32} over our temperature range 1048–473 °K, but our fit is not sufficiently sensitive to such a small effect to permit a determination of the temperature dependence. The value $K_{32} \simeq 9.8\times10^{-31}$ cm^6 sec^{-1} probably represents the actual rate at some mean temperature around 700 °K. This value seems quite reasonable since it is a factor of 6 larger than the dimer formation rate at 673 °K, $K_0^{(3)} \simeq 1.6\times10^{-31}$ cm^6 sec^{-1}. The trimer formation rate is expected to be about this much greater because the trimers are formed from dimers which have a collision diameter two or three times larger than the atoms from which dimers are formed.

The rate coefficient for trimer destruction k_{23} may not be interpreted as a simple binary collision rate coefficient which can be cast in the form $v\sigma$. A velocity $v \simeq 10^4$ sm sec^{-1} would correspond to an enormous cross section $\sigma \simeq 1.7\times10^{-12}$ cm^2, or about 300 times greater than any reasonable estimate of a gas kinetic cross section. Rather, the coefficient k_{23} should be regarded as the pre-exponential factor in an Arrhenius expression [recall that $R_{23} = g_2 n k_{23} \exp(-E_{23}/kT)$], which is obtained by solving the set of coupled equations for vibrational states which are needed to describe the collisional dissociation of a molecule. These equations have been solved by Nikitin[13] (see also pp. 271–275 of Ref. 12) and the solution used to calculate pre-exponential factors for collisional dissociation of several different types of molecules [see Table 20(a), p. 275 of Ref. 12, noting that A/Z_0 is the ratio of the pre-exponential factor A to the corresponding gas kinetic rate Z_0]. It is found that this pre-exponential factor for polyatomic molecules is typically 50 to 1000 times greater than the corresponding gas kinetic rate. Thus, it would seem that our value of k_{23} is also quite reasonable when compared to similar molecules but, due to uncertainties in the fit, it could still vary by as much as an order of magnitude.

The rate coefficient for collisions which couple the radiating 1_u state to the low lying metastable dimer state is $k_{21} \simeq 1.6\times10^{-10}$ cm^3 sec^{-1}. This corresponds to a collision cross section the order of 10^{-14} cm^2, which seems a bit large but again k_{12} should be regarded as a pre-exponential factor rather than a binary collision rate coefficient. A solution of the vibrational equations may again yield a value of k_{12} which agrees with our value.

The rate R_{13} could not be determined because it was usually added to R_{23} which is much larger [due to the exponential factors in Eqs. (3.16) and (3.17)], thus obscuring the effect of R_{13}.

The trimer formation rate from the 1_u state r_{31} was also very poorly fixed by the experimental data and varied from 10^{-34} to 3×10^{-31} cm^6 sec^{-1}. It was not included in Table I due to this rather large uncertainty.

The ratio $\phi \equiv K_{10}/(K_{10}+K_{20})$ is 0.3, indicating that the dimer formation rates for the radiating and metastable states are about the same, to within an order of magnitude.

The molecular parameters were determined primarily by the decay rates for high densities (Sec. IV.A) and the intensity ratio data (Sec. IV.C) and were thus affected very little by uncertainties in the atomic parameters discussed in the following section.

E. Atomic decay parameters

The atomic decay parameters were studied extensively in Ref. 6; however, these parameters were determined only at a temperature of 673 °K. It was noted that the atomic decay was roughly proportional to $1/T$ at a density of 2×10^{18} cm^{-3} (Fig. 7 of Ref. 6), but this observation was not sufficient to determine the temperature dependence of the individual rate coefficients.

The fluorescence decay rates reported in the present paper are controlled by the atomic decay for $n = 10^{17}$ cm^{-3}, where we have data from 923 to 473 °K (Fig. 6), and for low temperatures (mainly 473 °K), where we have data from 3×10^{16} to 10^{18} cm^{-3} (Fig. 7). These

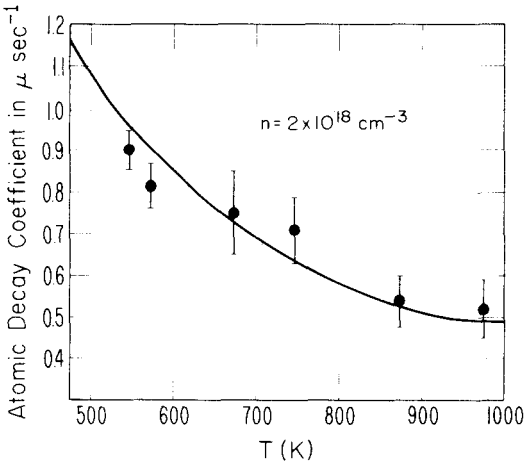

FIG. 13. Atomic decay coefficient measured at a density of 2×10^{18} cm^{-3} in Ref. 6. The solid curve represents our fit to the data using the theoretical expression given in Eq. (4.9).

new data, together with the temperature dependent data of Ref. 6, now permit a determination of the temperature dependence for some of the atomic decay parameters.

In analogy with Eq. (3.3) of Ref. 6 the atomic decay rate is expressed in the form

$$\gamma_0 = \frac{3\beta n(T/673)^a k_0^{(2)}}{\beta + n(T/673)^a k_0^{(2)}}\, e^{-\Delta E/kT} + n\left(\frac{T}{673}\right)^b k_q + n^2\left(\frac{673}{T}\right)^c K_0^{(3)}\,, \tag{4.9}$$

where $K_0^{(3)}$ is the three body molecular formation rate coefficient at 673 °K, k_q is the quenching rate coefficient at 673 °K, $k_0^{(2)}$ is the binary collision rate coefficient for $^3P_1 \rightarrow {}^3P_0$ transitions at 673 °K, $\Delta E = 1690$ cm^{-1} is the energy spacing between the $^3P_1$ and $^3P_0$ levels, and β is the radiative loss rate for the $^3P_1$ state which includes the effect of radiation trapping. The general expression[14] for β is a very complicated function of density but, in our case, β is important only for $n = 10^{17}$ cm^{-3}, hence, β will be regarded as a simple constant. Losses due to atomic diffusion were evaluated using the known diffusion rate[9,10,15] and found to be negligible for the present experimental geometry. The parameters β, $k_0^{(2)}$, k_q, $K_0^{(3)}$, a, b, and c were treated as adjustable constants and were determined by fitting the molecular fluorescence decay (Fig. 6) at low densities (mainly 10^{17} cm^{-3}) and low temperatures (Fig. 7), as well as the atomic decay data at $n = 2\times10^{18}$ cm^{-3} obtained from Fig. 7 of Ref. 6 (the latter are plotted, together with out fit, in Fig. 12 of the present paper). In these fits the molecular parameters were held fixed at the values determined in the preceding section.

The three body rate coefficient $K_0^{(3)}$ and its temperature dependence are well determined by the low temperature fluorescence data, (Fig. 7), and the high density atomic decay data (Fig. 13). The value of 1.8×10^{-31} cm^6 sec^{-1} agrees very closely with the value 1.6×10^{-31} cm^6 sec^{-1} obtained in Ref. 6 and the $(1/T)^{1.4}$ temperature dependence is consistent with that observed for other molecules (Ref. 12, p. 336).

The value $\beta = 2.5\times10^4$ sec^{-1} is very close to the theoretical value 2.8×10^4 sec^{-1} obtained using the theoretical results of Walsh[14] for $n = 10^{17}$ cm^{-3} and a cylindrical geometry of 2 mm, diameter (the diameter of our pump laser beam). This value also agrees to within the expected accuracy with the value 10^4 sec^{-1} obtained in Ref. 6.

The $^3P_1 \rightarrow {}^3P_0$ collisional rate coefficient $k_0^{(2)} = 1.5\times10^{-13}$ cm^3 sec^{-1} agrees to within a factor of 2 with the value 2.8×10^{-13} cm^3 sec^{-1} obtained in Ref. 1 and lies within the range of values obtained by Waddel and Hurst.[15] The fit to the data was essentially uneffected by a rather wide range of values for the coefficient a (temperature dependence of $k_0^{(2)}$; hence, this parameter was undetermined).

The quenching rate k_q was too small to be determined accurately; nonetheless, it was possible to set an upper bound of 5×10^{-15} cm^3 sec^{-1} for it. This is an order of magnitude smaller than the value obtained in Ref. 6. A larger value of k_q, say $k_q \simeq 10^{-14}$ cm^3 sec^{-1}, with a $(T/673)^{5/2}$ temperature dependence would have improved the agreement with the high density atomic decay (Fig. 13). Such a value slightly worsens the fit to the low density fluorescence data in Fig. 6 by adding about 10^3 sec^{-1} to the theoretical values of γ. This adds one unit to the $n = 10^{17}$ cm^{-3} curve which raises it slightly above the experimental data; this is not a serious discrepancy considering the accuracy of the data for 10^{17} cm^{-3}. On the other hand, if we use the larger values for k_q and $K_0^{(3)}$ in comparing with the atomic decay data (Fig. 6 of Ref. 6), the theoretical curve is again raised only slightly above the data points for high densities ($n \geq 5\times10^{18}$ cm^{-3}) and is slightly low for intermediate densities (8×10^{17}–10^{18} cm^{-3}). In short, the data are not sufficiently sensitive to k_q to determine its value to within an order of magnitude.

[1] R. E. Drullinger, M. M. Hessel, and E. W. Smith, J. Chem. Phys. **66**, 5656 (1977).
[2] E. W. Smith, R. E. Drullinger, M. M. Hessel, and J. Cooper, J. Chem. Phys. **66**, 5667 (1977).
[3] P. J. Hay and T. H. Dunning, J. Chem. Phys. **65**, 2679 (1976); and F. Mies, M. Krauss, and W. J. Stevens, submitted to J. Mol. Spectrosc.
[4] E. R. Mosburg and M. Wilke, J. Chem. Phys. **66**, 5682 (1977).
[5] C. G. Matland and A. O. McCoubrey (unpublished Westinghouse Research Memo).
[6] M. Stock, E. W. Smith, R. E. Drullinger, and M. M. Hessel, J. Chem. Phys. **67**, 2463 (1977).
[7] T. W. Hansch, Appl. Opt. **11**, 895 (1972).
[8] R. E. Drullinger, M. M. Hessel, and E. W. Smith, Natl. Bur. Stand. Monogr. **143** (1975).
[9] A. O. McCoubrey, Phys. Rev. **93**, 1249 (1954).
[10] N. P. Penkin and T. P. Redko, Opt. Spectrosc. **36**, 132 (1974).
[11] M. Abramowitz and I. A. Stegun, "Handbook of Mathematical Functions," Natl. Bur. Stand. Appl. Math. Ser. **55** (1964), p. 17.
[12] V. N. Kondrat'ev, *Chemical Kinetics of Gas Reactions* (Pergamon, Addison-Wesley, 1964).
[13] E. E. Nikitin, Sov. Phys. Dokl. **3**, 701 (1958); E. E. Nikitin and N. D. Sokolov, J. Chem. Phys. **31**, 1371 (1959).
[14] P. J. Walsh, Phys. Rev. **116**, 511 (1959).
[15] B. V. Waddell and G. S. Hurst, J. Chem. Phys. **53**, 3892 (1970).